Center for Turbulence Research
Proceedings of the Summer Program 1987

Big Whorls Carry little whorls

By J.C.R. Hunt[1], J.C. Buell[2], and A.A. Wray[2]

The space-time structure of homogeneous isotropic turbulence has been studied using a direct spectral simulation on a 64^3 mesh at a microscale Reynolds number of $Re_\lambda = 48$. Steady body forces were applied to a few low-wavenumber modes to make the flow statistically stationary. The results for the two-point space-time correlations of velocity and pressure (R_{11} and R_{pp}) show that the auto-correlations of u and p are positive and have about the same integral time scales, and that the spatial correlation $R_{pp}(r) \simeq R_{11}(0,r,0)$. The form of $R_{pp}(r)$ and the result that $\overline{p^2}/(\rho u_0^2)^2 \simeq 1.0$ agree fairly well with the Hinze/Batchelor (Hinze 1975) results. The three-dimensional energy spectrum for small space-time scales of velocity and pressure are consistent with the concept of large eddies advecting the small scales with a random Gaussian velocity (rms value of one component is u_0): the wavenumber (k), frequency (ω) and the energy spectrum $\mathcal{E}(k,\omega)$ are related to the spatial energy spectrum $E(k)$ by the formula

$$\mathcal{E}(k,\omega) = E(k)\exp\left[-\tfrac{1}{2}\omega^2/(aku_0)^2\right]/(\sqrt{2\pi}(aku_0)),$$

where $a \simeq 0.4$-0.5. The same form is found for the pressure spectrum. Extrapolating this result to high Reynolds number implies that in the inertial range the frequency spectra are $\phi_{11}(\omega) \propto (\epsilon u_0)^{2/3}\omega^{-5/3}$ (Tennekes 1975), and $\phi_{pp}(\omega) \propto (\epsilon u_0)^{4/3}\omega^{-7/3}$.

1. Introduction

1.1 Background to the project

Recent reports on the structure of turbulence and its dynamics have tended to emphasize the representation and the dynamics of the *spatial* structure rather than the temporal structure of the turbulent velocity field. However, closer examination of dynamical theories (e.g., Kraichnan's, described by Leslie 1981) show that they are always based on certain assumptions about the temporal structure, which have not been subjected to detailed examination or computation.

The temporal structure of turbulence also needs to be understood in order to develop models for the effects of turbulence and fluctuating pressure fields on the generation of surface and internal waves (Carruthers & Hunt 1986) and on dispersion of pollutants, particles and bubbles. One of the ways of developing practical models for these problems is first to develop a stochastic representation of the velocity field.

1 University of Cambridge
2 NASA Ames Research Center

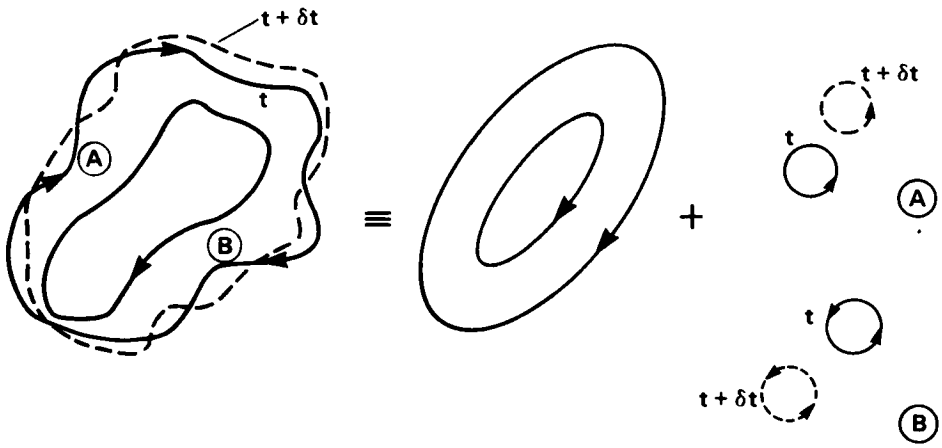

FIGURE 1. Flow field composed of large scale eddies and small scale eddies that are transported by the large scales. The small eddies also deform on a larger time scale.

The current research on the *spatial* structures (such as that of Moin 1987 and Moin, Adrian & Kim 1987) needs to be supplemented by information on how the turbulent velocity field evolves in *time*. (Some initial suggestions were put forward by Turfus & Hunt 1986, but they will be superceded by the present work.)

The clearest recent account of the temporal structure of turbulence is given by Tennekes (1975) and Tennekes & Lumley (1979). Essentially, the current understanding is that the largest scales of turbulence with velocity and length scales u_0 and L are unsteady and change on a time scale L/u_0. Meanwhile, smaller eddies on a scale ℓ with velocity $u(\ell)$ (defined by the structure function $\overline{[|\mathbf{u}(\mathbf{x}) - \mathbf{u}(\mathbf{x}+\mathbf{r})|^2]}^{1/2}$, where $|\mathbf{r}| = \ell$), have two time scales: the Eulerian time scale

$$\tau_E(\ell) \sim \ell/u_0, \tag{1.1a}$$

for the eddy to be advected by the large eddies past an observing point (moving with the mean flow), and the Lagrangian time scale

$$\tau_L(\ell) \sim \ell/u(\ell), \tag{1.1b}$$

for the velocity field on a scale (ℓ) to change as it is advected by the large scale eddies. See figure 1.

Thus at a point (moving with the mean flow), the dominant time-dependent phenomenon (which determines $\partial\mathbf{u}/\partial t$) is the rapid, random movement of small scale eddies past the observer by the large eddies. On the other hand, for a point moving *with the fluid*, the only change of velocity is the slow change caused by the dynamical processes at the scale ℓ. These differences are best defined by the *Eulerian* microscale

$$\tau^{(E)} = \left[\overline{(\partial\mathbf{u}/\partial t)^2}\Big/\overline{\mathbf{u}^2}\right]^{-1/2}, \tag{1.2a}$$

and the *Lagrangian* microscale, following a material element,

$$\tau^{(L)} = \left[\overline{(d\mathbf{u}/dt)^2}\Big/\overline{\mathbf{u}^2}\right]^{-1/2}. \tag{1.2b}$$

For high Reynolds number turbulence these can be related to the basic time scale L/u_0 by

$$\tau^{(E)} \sim Re^{-1/2}L/u_0, \tag{1.3a}$$

and

$$\tau^{(L)} \sim Re^{-1/4}L/u_0, \tag{1.3b}$$

where $Re = u_0L/\nu$. Tennekes (1975) found that these estimates were consistent with the grid turbulence measurements of Shlien & Corrsin (1974). Another important consequence of Tennekes's analysis is that for high Reynolds number turbulence in the inertial subrange, the frequency spectrum $\phi_{11}(\omega)$ of one component of the velocity, say u_1, measured at a point (moving with the mean flow) has a form which is different from the universal Lagrangian form

$$\phi_{11}^{(L)}(\omega) = C_\omega^L \epsilon \omega^{-2}, \tag{1.4a}$$

namely

$$\phi_{11}^{(E)}(\omega) = C_\omega^E (\epsilon u_0)^{2/3}\omega^{-5/3}, \tag{1.4b}$$

where C_ω^E is a constant for a given flow. Since this form depends on the large scales which do not have (even approximately) a universal character, it is not likely that C_ω^E is a universal constant, unlike the constant for the one-dimensional wavenumber spectrum $\phi_{11}(k_1)$ or energy spectrum $E(k)$. The prediction (1.4b) has not to our knowledge been properly tested experimentally or computationally.

No detailed analyses have been developed for the four-dimensional wavenumber-frequency spectrum tensor $\Psi_{ij}(\mathbf{k},\omega)$ or its equivalent energy spectrum $\mathcal{E}(k,\omega)$, defined by

$$\Psi_{ij}(\mathbf{k},\omega) = \frac{1}{(2\pi)^4}\int\int\int\int \overline{u_i(\mathbf{x},t)u_j(\mathbf{x}+\mathbf{r},t+\tau)}e^{i(\mathbf{k}\cdot\mathbf{r}+\omega\tau)}d\mathbf{r}d\tau, \tag{1.5a}$$

and

$$\mathcal{E}(k,\omega) = \int_{|\mathbf{k}|=k} \Psi_{ii}(\mathbf{k},\omega)dA(\mathbf{k}). \tag{1.5b}$$

Note that

$$E(k) = \int_{-\infty}^{\infty} \mathcal{E}(k,\omega)d\omega. \tag{1.5c}$$

However, Carruthers & Hunt (1986) made a rash speculation based on Tennekes's time scale argument (in order to estimate internal wave generation) that

$$\Psi_{ij}(\mathbf{k},\omega) \simeq \Phi_{ij}(\mathbf{k})\delta(\omega \pm ku_0), \qquad \text{where} \qquad \Phi_{ij}(\mathbf{k}) = \int_{-\infty}^{\infty} \Psi_{ij}(\mathbf{k},\omega)d\omega. \tag{1.6}$$

Measurements have been made of one-dimensional space-time correlations $R(r,\tau)$ of velocity and pressure fluctuations in grid turbulence and in boundary layers (Favre *et al.* 1956; Wills 1971), and in a pipe (Sabot & Comte-Bellot 1976). The general features have been described by formulae of the form (in coordinates moving with the mean flow)

$$R_{11}(r_1,\tau) \simeq R_{11}(r)F(\tau,r,u_0,L)$$

where $F(\tau=0)=1$, and F decreases with r more slowly as τ increases. See Hinze (1975 p. 416). Similar forms are observed for fluctuating pressure. Wills (1971) also took the Fourier transform of these measurements and calculated the one-dimensional wavenumber-frequency spectra $\phi_{pp}(k_1,\omega)$. When converted into a frame moving at the same mean speed as the travelling pressure field, he found that his result could be expressed as

$$\phi_{pp}(k_1,\omega) = \phi(k_1)f\Big(\frac{\omega}{k_1u_0}\Big), \tag{1.7}$$

where $f \simeq \exp\big(-\frac{1}{2}\frac{\omega^2}{k_1^2u_0^2}\big)$, and u_0 is the rms value of the streamwise velocity component (at $y/\delta \simeq 0.5$). Moser & Moin (1984) computed space-time correlations for channel flow.

An interesting quantity that can be derived from these correlations is the Eulerian time scale $T_{ii}^{(E)}$ (in a frame moving with the mean flow) of the i^{th} velocity component. [Since the measurements are not extensive enough for $T^{(E)}$ to be computed from *integrals* of $R_{11}(\tau)$, $T^{(E)}$ has to be estimated from the value of τ at which $R_{11} \simeq 1/e$.] The results of Favre and Moser & Moin indicate that the value of $T_{ii}^{(E)}$, normalized in terms of the rms velocity and the integral length scale L_1^{ii} in the flow direction has a range of values given by

$$\beta^{(E)} = T_{ii}^{(E)}\sqrt{\overline{u_i^2}}\Big/L_1^{ii}, \tag{1.8}$$

where $1 \le \beta^{(E)} \le 2$. Snyder & Lumley (1971) inferred a value of $\beta^{(E)} \simeq 3$ from their measurements of small particles in grid turbulence.

Using the same normalization for the Lagrangian integral time scale $T_{ii}^{(L)}$, defined by

$$\beta^{(L)} = T_{ii}^{(L)}\sqrt{\overline{u_i^2}}\Big/L_1^{ii}, \tag{1.9}$$

experiments and simulations indicate that $\beta^{(L)} \simeq 1$ for grid turbulence (Snyder & Lumley 1971), and boundary layer turbulence (Durbin & Hunt 1980). A random Fourier mode representation for homogeneous turbulence has produced a value of $\beta^{(L)} \simeq 1/3$-$1/2$.

So the current position is that the magnitudes of $\beta^{(E)}$ and $\beta^{(L)}$ are *not* well defined.

1.2 Aims of the project

The aim of the research presented here is to explore the space-time structure of homogeneous turbulence by computing and then interpreting the two-point spectra and correlations of the velocity and pressure fields. Many of these statistics are of considerable practical importance, as indicated in the previous section. In particular it is of interest to compare the different time and length integral scales and microscales for Eulerian and Lagrangian quantities, and to compare the space and time spectra.

2. Some Theoretical Ideas for Guiding Interpretation

2.1 Velocity spectra

2.1.1 Simple non-interacting eddies

Consider a set of smooth eddies on a line, each located at a position x_n, with a spatial scale ℓ_n, a turnover time ω_n^{-1}, and a random phase ϵ_n. We consider, for simplicity, one component of turbulence, u_1; then a typical form for u_1 is

$$u_1(x,t) = \sum_{n=0}^{N} a_n \exp\left[-\frac{(x-x_n)^2}{2\ell_n^2}\right] \cos(\omega_n t + \epsilon_n), \tag{2.1}$$

where a_n are random amplitude coefficients which are independent, $\overline{a_n a_m} = \delta_{nm}\overline{a_n^2}$. We assume the mean of ω_n is $\overline{\omega_n}$, and its random element has variance $\sigma^2_{\omega_n}$.

The cross correlation at points x and $x+r$ and times t and $t+\tau$, when averaged over a length $X \sim \sum \ell_n$ and over a sufficiently long time, is

$$R_{11}(r,\tau) = \frac{\sqrt{\pi}}{2X} \sum_{n=0}^{N} \overline{a_n^2}\ell_n \exp\left(-\frac{r^2}{4\ell_n^2}\right) \exp(-\tfrac{1}{2}\sigma^2_{\omega_n}\tau^2) \cos(\overline{\omega_n}\tau). \tag{2.2a}$$

So in general the space-time correlation is not simply related to the spatial correlation $R_{11}(r)$. But, for the case of just one eddy scale L, where $N = 0$, R_{11} reduces to

$$R_{11}(r,\tau) = \frac{\sqrt{\pi}}{2X} a_0^2 L \exp\left(-\frac{r^2}{4L^2}\right) \exp(-\tfrac{1}{2}\sigma^2_{\omega_0}\tau^2) \cos(\omega_0\tau), \tag{2.2b}$$

or

$$R_{11}(r,\tau) = R_{11}(r,\tau=0) f(\tau).$$

Then the time and space correlations are separable. Similarly the wavenumber and frequency spectra are not linked, for this type of flow field.

2.1.2 Small eddies moved by a large-scale velocity field

Now consider a set of small eddies moved by a random large scale velocity U. These might be the small scale components of turbulent flow. Again, take one dimension: Let

$$u = \sum_{m=-M}^{M} \sum_{n=-N}^{N} a_{nm} \exp\left[i(k_n x + \omega_m t)\right], \tag{2.3}$$

where $\omega_m = Uk_m + \omega'_m$, a_n is again a set of random amplitude coefficients, and ω'_m is the frequency in the advected frame.

Let the probability density function of U be $p(U)$. Then

$$R_{11}(r,\tau) = \int \sum_{m=-M}^{M} \sum_{n=-N}^{N} |a_{nm}^2| \exp\left[i(k_n r + k_n \tau U + \omega'_m \tau)\right] p(U) dU. \tag{2.4}$$

It is interesting to consider two possibilities for $p(U)$.

(a) $p(U)$ is Gaussian with variance U_0^2:

$$R_{11}(r,\tau) = \sum_{m=-M}^{M} \sum_{n=-N}^{N} |a_{nm}^2| e^{ik_n r} e^{-\frac{1}{2}\tau^2 k_n^2 U_0^2} e^{i\omega'_m \tau}. \tag{2.5}$$

Then the one-dimensional wavenumber frequency spectrum is

$$\begin{aligned}\psi(k_1,\omega) &= \frac{1}{(2\pi)^2} \sum_{m=-M}^{M} \sum_{n=-N}^{N} \int_{-\infty}^{\infty} |a_{nm}^2| e^{i(k_n - k_1)r} dr \int_{-\infty}^{\infty} e^{(-\frac{1}{2}\tau^2 k_n^2 U_0^2 - i(\omega - \omega'_m)\tau)} d\tau \\ &= \sum_{m=-M}^{M} |a_{k_1 m}|^2 \exp\left[-\frac{(\omega - \omega'_m)^2}{2k_1^2 U_0^2}\right] \Big/ (\sqrt{2\pi}|k_1|U_0).\end{aligned} \tag{2.6}$$

For high wavenumbers, the advective time scale $(k_1 U_0)^{-1}$ is much less than the time scale for the eddies to change as they move. Consequently $|\omega'_m| \ll |k_1 U_0|$. By taking large enough values of N to give a dense distribution of Fourier modes, a spatial spectrum $\phi(k_1)$ from $\psi(k_1,\omega)$ can be defined. From (2.6),

$$\psi(k_1,\omega) = \phi(k_1) \exp\left(-\frac{\omega^2}{2k_1^2 U_0^2}\right) \Big/ (\sqrt{2\pi}|k_1|U_0). \tag{2.7}$$

Note that

$$\overline{u^2} = \int_{-\infty}^{\infty} \phi(k_1) dk_1 = \int_{-\infty}^{\infty} \int_{-\infty}^{\infty} \psi(k_1,\omega) dk_1 d\omega. \tag{2.8}$$

In a three-dimensional isotropic velocity field, $\omega_n = \mathbf{U} \cdot \mathbf{k}_n + \omega'_n$, and for a Gaussian distribution of the 3-D large-scale velocity $\mathbf{U}$, it can be shown that the relation between the k-ω energy spectrum and the k energy spectrum is

$$\mathcal{E}(k,\omega) = E(k) \exp\left(-\frac{\omega^2}{2k^2 U_0^2}\right) \Big/ (\sqrt{2\pi} k U_0), \tag{2.9}$$

where $U_0^2 = \frac{1}{3}\overline{|\mathbf{U}|^2}$.

(b) The large-scale velocity has a constant magnitude (forwards or backwards):

In this case $p(U) = \frac{1}{2}\left[\delta(U - U_0) + \delta(U + U_0)\right]$, and this leads to

$$R_{11}(r,\tau) = \sum_{n} |a_n^2| e^{ik_n r} e^{i\omega_{n0}\tau} \cos(\tau k_n U_0),$$

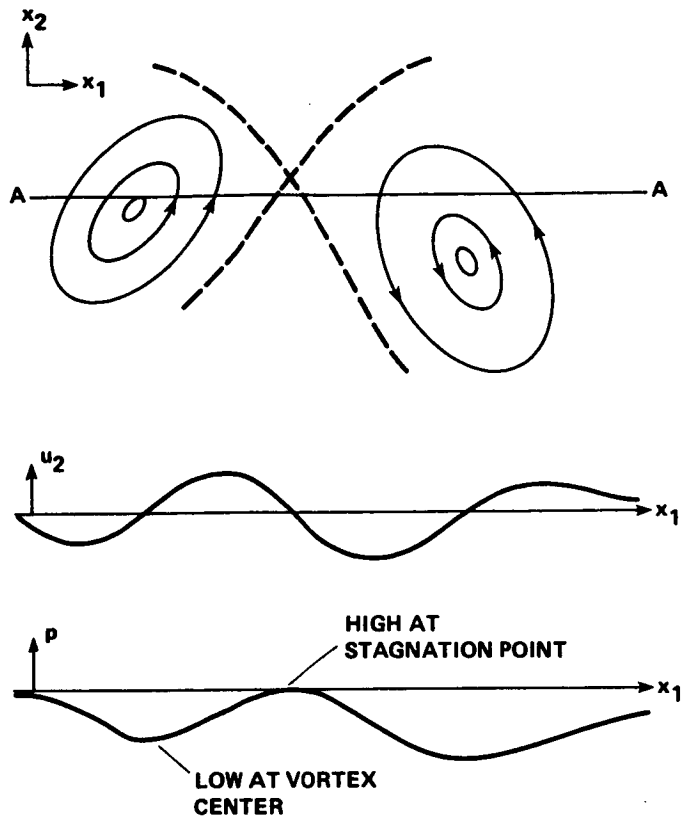

FIGURE 2. Similarity of the length scales of velocity and pressure fields induced by large vortices.

and

$$\psi(k_1,\omega) = \phi(k_1)\frac{1}{2}\left[\delta(\omega - k_1U_0) + \delta(\omega + k_1U_0)\right]. \tag{2.10}$$

2.2 Pressure

For large eddies having a form similar to vortices (such as analyzed by Townsend 1976), the large scale distribution of pressure across the eddy, say in the x_1 direction, has a distribution similar to that of $u_2(x_1)$ (figure 2). Consequently, the pressure correlation $R_{pp}(r_1)$ is expected to have the same scale and form as $R_{22}(r_1)$.

The pressure fluctuations at small scales have been found in previous investigations (e.g. George *et al.* 1982) to be *caused* by the motions of eddies on that scale, and not (for example) by interactions between small scales and large scales. The former (which is observed) gives $\phi_{pp}(k_1) \propto \epsilon^{4/3}k_1^{-7/3}$, while the latter gives $\phi_{pp}(k_1) \propto (U_0^2/L^2)\epsilon^{2/3}k_1^{-11/3}$. Thus it is expected that, as the large scale eddies *advect* the small eddies, they also advect the small scale pressure fluctuations. Therefore the k-ω power spectrum of pressure fluctuations is *expected* to have the

form

$$\mathcal{E}_{pp}(k,\omega) = E_{pp}(k)\exp\left(-\frac{\omega^2}{2k^2U_0^2}\right)\Big/(\sqrt{2\pi}kU_0). \tag{2.11}$$

This is close to the values measured by Wills (1971).

3. Method

To obtain the frequency spectra and time correlation of a turbulent velocity field, a long time record is necessary; a decaying turbulent field is not appropriate because the amplitude decay does not allow a long enough time record. It is necessary to generate a statistically stationary velocity field.

The method used in these computations is to introduce a *steady* nonuniform force field $\mathbf{F}(\mathbf{x})$ at the largest scale of the flow (defined to be 2π in all three directions), which induces a mean flow at this scale. The mean flow is unstable, allowing instabilities to grow. This leads to a chaotic structure with motions at all scales down to the Kolmogorov microscale. If the initial conditions are chaotic, the force field will maintain the turbulence, but not necessarily at the original amplitude. Given a spatially periodic flow (whose maximum scale is fixed) any steady force distribution will eventually give rise to a stationary turbulent flow. This flow is determined by $\mathbf{F}$ and the viscosity ν.

The computations were performed on a $N_x \times N_y \times N_z$ mesh with periodic boundary conditions. The force spectrum $E_f(k)$ is chosen to have contributions from values of $k = \sqrt{2}$, i.e., $\mathbf{k} = (\pm1, 0, \pm1)$, $(\pm1, \pm1, 0)$, and $(0, \pm1, \pm1)$. To generate isotropic turbulence, all the moments of the body force $\mathbf{F}(\mathbf{x})$ would have to satisfy isotropy conditions. This could only be done approximately, by ensuring that moments up to second order of the Fourier coefficients of $\mathbf{F}$, $\hat{\mathbf{f}}$, satisfied isotropy. We also specified that $\overline{\hat{f}_1\hat{f}_2\hat{f}_3} = 0$. $\mathbf{F}$ was chosen to be solenoidal to avoid the generation of large pressure fluctuations. For each $\mathbf{k}$ such that $|\mathbf{k}| = \sqrt{2}$ the amplitude of the forcing was set so that $\sqrt{\hat{f}_i(\mathbf{k})\hat{f}_i^*(\mathbf{k})} = 0.2$. The viscosity ν was .02.

The 3-D Navier-Stokes equations were solved under the above conditions using the spectral code of Rogallo (1981) modified to include the body force $\mathbf{F}$. The primary results of the computation were the time-dependent, 3-D spatial Fourier coefficients of the velocity, $\hat{\mathbf{u}}$, and pressure, $\hat{p}$, fields, defined by

$$u_j(\mathbf{x},t) = \sum_{k_1=-N_x/2}^{N_x/2}\ \sum_{k_2=-N_y/2}^{N_y/2}\ \sum_{k_3=-N_z/2}^{N_z/2} \hat{u}_j(\mathbf{k},t)\exp(i\mathbf{k}\cdot\mathbf{x}), \tag{3.1}$$

where $N_x = N_y = N_z = 64$. A similar definition applies to $\hat{p}(\mathbf{k},t)$.

After storing $\hat{u}_j(\mathbf{k},t)$ at M time intervals Δt_s, the individual time series are filtered with a cosine "window" within the period $T = M\Delta t_s$. Fourier transforms in time yield the 3-D space-time Fourier coefficients $\hat{\hat{u}}_j(\mathbf{k},\omega_m)$, defined by

$$\hat{u}_j(\mathbf{k},t) = \sum_{m=-M/2}^{M/2} \hat{\hat{u}}_j(\mathbf{k},\omega_m)\exp(i\omega_m t), \tag{3.2}$$

where $\omega_m = 2\pi m/T$.

The time interval Δt_s used for the computation of frequency spectra and time correlations must be small enough to resolve the shortest time variation *at a point.* This minimum Eulerian time scale $\tau_{\min}^{(E)}$ is defined by the fast large eddies carrying, at a velocity u_0, the smallest scale eddies ℓ_{Kol} past the point, i.e., $\tau_{\min}^{(E)} \sim \ell_{\text{Kol}}/u_0$. (It is $Re_\lambda^{-1/2}$ times the magnitude of the Eulerian microscale!) In our computations Δt (based on CFL limitations) turned out to be less than $0.1\tau_{\min}^{(E)}$, thus we took $\Delta t_s = 10\Delta t$.

The flow was initiated by suddenly imposing the force field on a given initial random isotropic velocity field $\mathbf{u}(\mathbf{x}, t=0)$. It was found that $\overline{u_j^2}$ initially increased or decreased, but eventually oscillated with small amplitude about a stationary value; then the time series were collected to obtain the statistics.

From the Fourier coefficients, space-time spectra and correlations may be computed, using the normalized length (2π) of the box.

(i) The wavenumber-frequency $(\mathbf{k}, \omega)$ energy spectrum tensor,

$$\Psi_{ij}(\mathbf{k}, \omega) = \overline{\hat{u}_i(\mathbf{k}, \omega)\hat{u}_j^*(\mathbf{k}, \omega)}, \tag{3.3}$$

and similarly for $\Psi_{pp}(\mathbf{k}, \omega)$.

(ii) The energy spectrum tensor,

$$\Phi_{ij}(\mathbf{k}) = \overline{\hat{u}_i(\mathbf{k}, t)\hat{u}_j^*(\mathbf{k}, t)}. \tag{3.4}$$

(iii) The energy spectra (summing over spherical shells in wavenumber space; the equivalent integral expressions for a continuum of wavenumbers are given in (1.5)),

$$\mathcal{E}(\bar{k}, \omega) = \sum_{\bar{k}-\frac{1}{2}<|\mathbf{k}|\leq\bar{k}+\frac{1}{2}} \Psi_{ii}(\mathbf{k}, \omega), \tag{3.5a}$$

$$E(\bar{k}) = \sum_{\bar{k}-\frac{1}{2}<|\mathbf{k}|\leq\bar{k}+\frac{1}{2}} \Phi_{ii}(\mathbf{k}). \tag{3.5b}$$

(iv) The one-dimensional space-time correlation,

$$R_{ij}(\mathbf{r}, \tau) = \sum_{\mathbf{k}} \sum_{m} \Psi_{ij}(\mathbf{k}, \omega) e^{i(\mathbf{k}\cdot\mathbf{r}+\omega_m\tau)}. \tag{3.6}$$

(v) One-dimensional spectra,

$$\Theta_{ij}(k_1, \omega) = \sum_{k_2} \sum_{k_3} \Psi_{ij}(\mathbf{k}, \omega). \tag{3.7}$$

4. Results of the computations

Table 1 gives most of the major statistics of the computed turbulent flow. Note that the Reynolds number based on the Taylor microscale, λ, is only 48, so that we

do not expect to see many features of high Reynolds number turbulence. However the Reynolds number is large enough so that the effects of *advection* of small scales can be investigated. Note also that the turbulent velocity field is not quite isotropic; the lack of isotropy in the moments ($\overline{u_1^2}/\overline{u_2^2} \simeq 1.1$) for a given realization is of the same order as that usually found in wind tunnel experiments. This probably means that the forcing is not quite isotropic. The ratio of the integral scales L'_{11}, L'_{22}, computed from the one-dimensional correlations $R_{11}(r_1,0,0)$, $R_{22}(r_1,0,0)$, is 1.64. This is less than the value of 2.0 required by isotropy. By comparison the *decaying* strained turbulence computed on a 128^3 mesh by Rogallo (1981) and others was effectively defined to be isotropic at its initiation.

Figure 3 shows the unfiltered and filtered time variations of typical large scale and small scale Fourier coefficients. Note the rather sudden changes in the small scale filtered velocity. The time scale τ_k for such a change is consistent with large scales advecting the small scales $(\tau_k \sim 2\pi/(u_0 k))$.

Figure 4a shows the contours of the energy spectrum $\mathcal{E}(k,\omega)$, and figure 4b the various statistics of the variation of $\mathcal{E}(k,\omega)$ with ω for different values of k. The mean and skewness are close to zero. The standard deviation defined by

$$\sigma_{\mathcal{E}} = \left[\int_{-\infty}^{\infty} \omega^2 \mathcal{E}(k,\omega)d\omega \Big/ \int_{-\infty}^{\infty} \mathcal{E}(k,\omega)d\omega\right]^{1/2} \tag{4.1}$$

is described by the formula $\sigma_{\mathcal{E}} = aku_0$, where $u_0 = \sqrt{\frac{1}{3}\overline{u_i^2}}$. The flatness (or kurtosis) is close to 3. Consequently $\mathcal{E}(k,\omega)$ can be approximated by

$$\mathcal{E}(k,\omega) = E(k)\exp\left[-\frac{\omega^2}{2(aku_0)^2}\right] \Big/ \left(\sqrt{2\pi}(aku_0)\right), \tag{4.2}$$

where $a \simeq 0.51$ for $kL_1 \leq 10$, and $a \simeq 0.4$ for $kL_1 \geq 15$ (figure 4c). A similar result for the k-ω energy spectrum for pressure has been found with $a_p \simeq 0.51$ for $kL_1 \leq 10$, and $a_p \simeq 0.45$ for $kL_1 \geq 15$. This result for $\mathcal{E}_{pp}(k,\omega)$ is in approximate agreement with the space-time correlation measurements of Wills (1971) for pressure fluctuations on the wall below a boundary layer.

An important consequence of (4.2) is that by assuming its validity at high Reynolds number we can *calculate* the Eulerian frequency spectra for the velocity $\phi_{11}(\omega)$ and the pressure $\phi_{pp}(\omega)$. Since $\phi_{11}(\omega) = \frac{1}{3}\int \mathcal{E}(k,\omega)dk$ and $E(k) = \alpha_k \epsilon^{2/3} k^{-5/3}$, where α_k is the Kolmogorov constant, we have

$$\phi_{11}(\omega) = \frac{\frac{1}{3}\Gamma(\frac{5}{6})a^{2/3}}{2^{2/3}\sqrt{\pi}} \alpha_k (\epsilon u_0)^{2/3} \omega^{-5/3}.$$

Taking $a = 0.51$ yields

$$\phi_{11}(\omega) = 0.085\alpha_k (\epsilon u_0)^{2/3} \omega^{-5/3}. \tag{4.3}$$

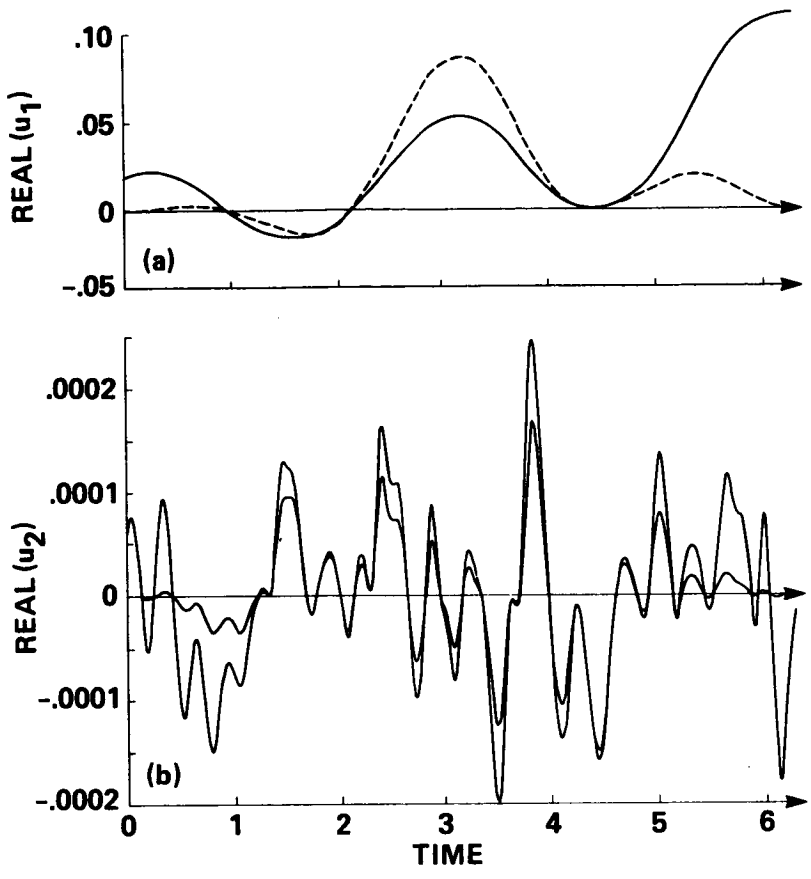

FIGURE 3. Typical time variation of computed Fourier coefficients over the period of time used for frequency calculations. The real part of $\hat{u}_i(k_x, k_y, k_z)$ is shown. The data is filtered to allow processing by discrete Fourier transform methods: the filtering is most apparent at the interval boundaries. (a) data at low wavenumber, $\hat{u}_1(1,1,1)$: —— unfiltered, ---- filtered; (b) filtered and unfiltered data at high wavenumber, $\hat{u}_2(4,4,19)$.

Similarly if $E_{pp}(k) = \alpha_{kp}\epsilon^{2/3}k^{-7/3}$ (George *et al.* 1984), we deduce that

$$\phi_{pp}(\omega) = \frac{\Gamma(\frac{7}{6})a_p^{4/3}}{2^{1/3}\sqrt{\pi}}\alpha_{kp}(\epsilon u_0)^{4/3}\omega^{-7/3}.$$

Taking $a_p = 0.51$ yields

$$\phi_{pp}(\omega) = 0.17\alpha_{kp}(\epsilon u_0)^{4/3}\omega^{-7/3}. \tag{4.4}$$

The result (4.3) has the same form as proposed by Tennekes (1975), while (4.4) appears to be new.

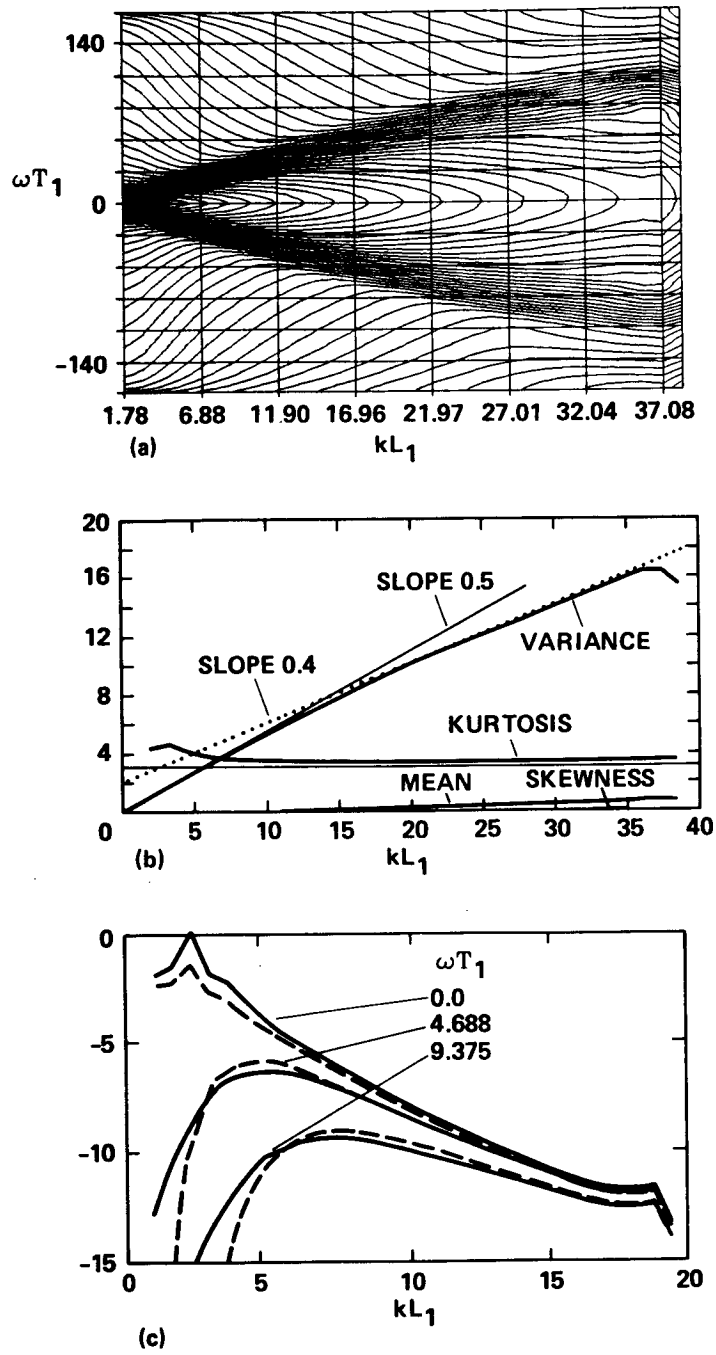

FIGURE 4. Space-time spectrum of energy. (a) Contours of the energy spectrum $\mathcal{E}(k,\omega)$. k is normalized on L_1, and ω on u_0/L_1. Contours are in factors of $\sqrt{10}$. (b) Moments of the frequency distribution of the energy spectrum. Note particularly the variance $\sigma_\mathcal{E}$ and the kurtosis $K_\mathcal{E}$. (c) Relation between the space-time spectrum and the space spectrum: —— $\mathcal{E}(k,\omega)$, - - - - (4.2). Results are from a later simulation.

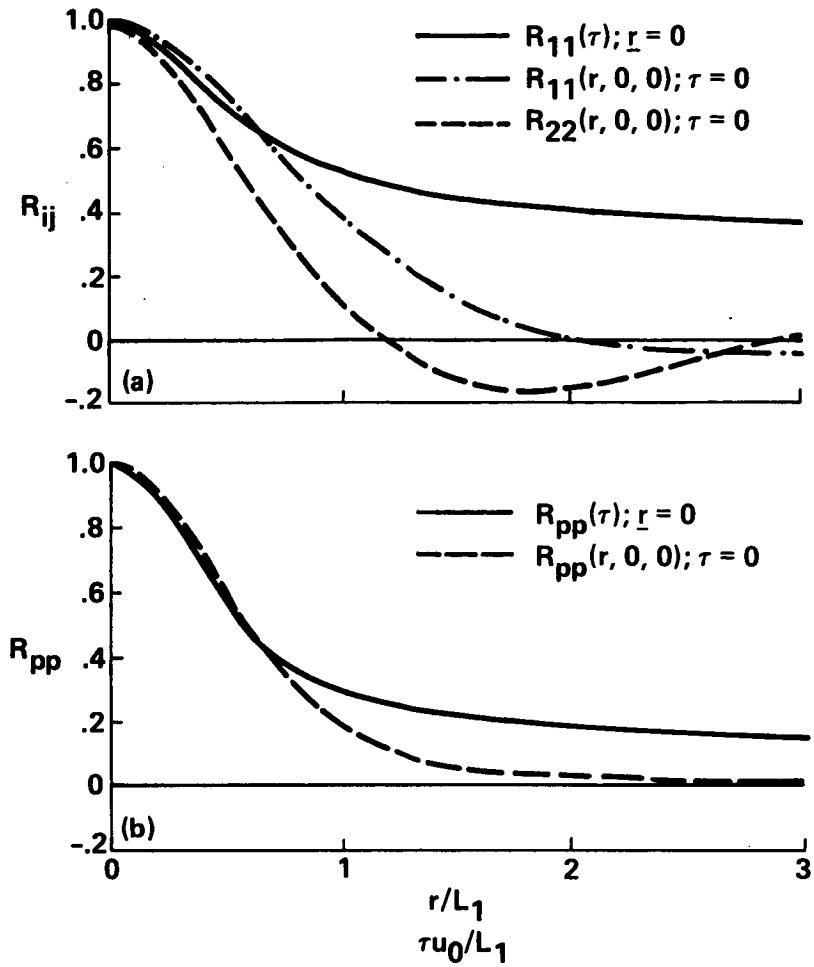

FIGURE 5. Auto-correlations in space and time for isotropic turbulence: (a) velocity, (b) pressure.

Figure 5 shows the longitudinal and transverse correlations of the velocity and pressure fields. Note that for the velocity, the auto correlation curve $R_{11}(\tau)$ has the same form as the longitudinal spatial correlation, $R_{11}(r_1)$, and is positive, at least for $r_1/L_1 \leq 2.5$. These curves are normalized on an integral length scale derived from the energy spectrum (Monin & Yaglom 1971, p. 55),

$$L_1 = \frac{3\pi}{4} \int_0^\infty k^{-1} E(k) dk \Big/ \int_0^\infty E(k) dk.$$

For these experiments $L_1/2\pi \simeq 0.25$, i.e., about a quarter of the box size. It is convenient to define length and time scales from these one-dimensional correlations by a similar procedure as in many experiments. Because of the finite box size, the one-dimensional integral scales are estimated from the value of the space or time variable where the correlation is $1/e$ of the variance. So $R_{11}(r = L_{11}^{(1)}) =$

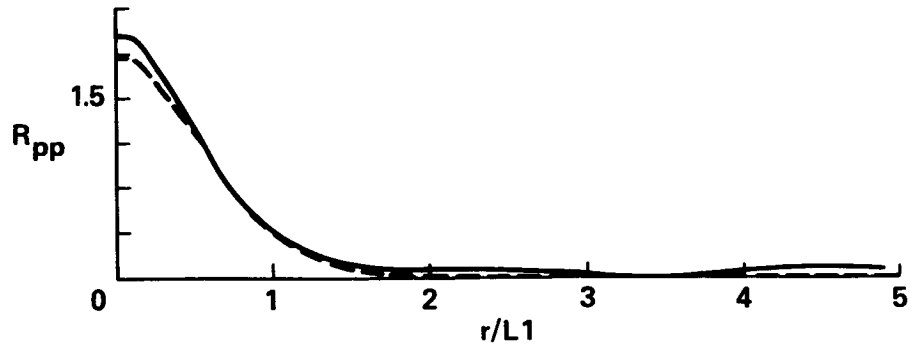

FIGURE 6. Comparison of the unnormalized pressure auto-correlation with the Hinze/Batchelor theory: —— computed, - - - - theory of Batchelor (1951). Results are from a later simulation.

$(1/e)R_{11}(r=0)$. On this basis our computed longitudinal length and time scales are

$$L_{11}^{(1)} = 1.25L_1,$$

and

$$T_1^{(E)} \simeq 1.5L_1/u_0.$$

This value of $T_1^{(E)}$ is greater than the value of $1.15L_1/u_0$ obtained by Kyle Squires (private communication) in *decaying* turbulence at $Re_\lambda = 35$. Both estimates are less than the value of 3 inferred by Snyder & Lumley (1971).

The pressure time and space correlations $R_{pp}(\tau)$ and $R_{pp}(r_1)$ are plotted in figure 5b. Note that $R_{pp}(r_1)/R_{pp}(0)$ has a similar form as $R_{22}(r_1,0,0)$ in that the curves become negative when $r/L_1 > 1.5$ for the former and $r/L_1 > 1.3$ for the latter. A plausible physical explanation can be based on the typical form of the large eddies discussed in §2.2. Note that, as for the velocity, the autocorrelation of the pressure fluctuations is positive. An important result is that the mean square pressure fluctuation is given by

$$\overline{p^2}/(\rho u_0^2)^2 \simeq 1.0.$$

This ratio is higher than the estimates made by Batchelor (1951) for low Reynolds number wind tunnel turbulence (0.34), and for high Reynolds number turbulence by Hinze (1975) (0.5), and George *et al.* (1984) (0.42).

A significant agreement with the theory of Batchelor (1951) is shown in figure 6 where the theoretical value of $R_{pp}(r_1)$ (using $R_{11}(r_1)$ from a later simulation having lower anisotropy) is compared with computational results. The agreement is quite good except near $r = 0$.

The final results, figure 7, were the power spectra E_1 to E_4 for the four quantities: $\nabla p + (\mathbf{u}\cdot\nabla)\mathbf{u}$, ∇p, $\frac{\partial \mathbf{u}}{\partial t}$, and $\frac{D\mathbf{u}}{Dt}$. For high Reynolds number turbulence, where the viscous terms are small, the first and third spectra should be equal and also the

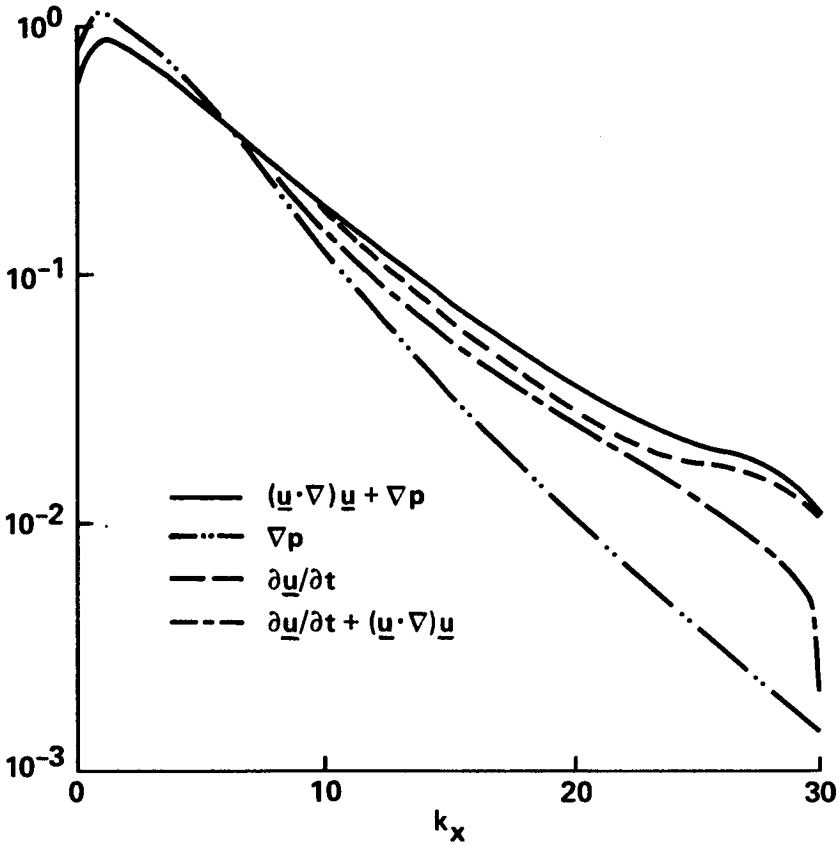

FIGURE 7. Power spectra of the terms in the Navier-Stokes equations.

second and fourth. Furthermore if the eddies are advected past an observer faster than they evolve by nonlinear or viscous processes, then following Tennekes (1975) $\frac{\partial \mathbf{u}}{\partial t}$ and $E_3(k)$ should be much greater than $\frac{D\mathbf{u}}{Dt}$ and $E_4(k)$ for large k. However the computations showed that E_3 and E_4 were of comparable magnitude (within 20%). But we did find that the ratio E_1/E_2 increased from about 1 to 8 as kL_1 increased from 8 to 36. This is consistent with the advective contribution to $(\mathbf{u}\cdot\nabla)\mathbf{u}$ being much greater than the local nonlinear contribution (which largely determines ∇p). We also found that E_4 (i.e. $\frac{D\mathbf{u}}{Dt}$) was about 2 or 3 times as great as E_2 (∇p), even for $kL_1 \simeq 20$, showing that the contribution of viscous stresses to E_4 and $\frac{D\mathbf{u}}{Dt}$ is dominant.

These viscous stresses are probably the explanation for why E_3 is of the same order as E_4. But if the viscous stresses are so relatively large, is this consistent with the small eddies being apparently advected by the large eddies? A possible explanation is that the small eddies are like slowly decaying vortices advected by the large eddies. Within the small eddies the viscous term $\nu\nabla^2\mathbf{u}$ may be *greater* than the advective acceleration term $(\mathbf{U}\cdot\nabla)\mathbf{u}$. But the time for the decay of say an extended line vortex with core size k^{-1} is *much longer* than $(\nu k^2)^{-1}$. Therefore we

draw the surprising conclusion that, for turbulence in this Reynolds number range, the locations of the viscous stresses is associated with relatively large values of $\frac{\partial u}{\partial t}$ suggesting that first there is not necessarily a local instantaneous balance between the large straining and dissipation, and second the small eddies decay as they are advected by the large eddies. Perhaps the generation of small scale turbulence occurs on *shorter time scales* than its decay.

5. Conclusions and Further Work

1. The central hypothesis to be tested in this project of large scale eddies (or Whorls) advecting (or carrying) small scale eddies (or whorls), was supported, if not completely confirmed. [Perhaps we should change one word in L.F. Richardson's rhyme: replace 'Big whorls *have* little whorls ...' with '... *carry* ... '!]

2. The computations raised numerous questions. To clarify the advection process we need to compute the probability distribution of the large eddies, and for the pressure correlations the probability distribution of the strain rates. We found that the pressure correlation agrees fairly well with the Hinze/Batchelor theory which is based on a quasi-normality assumptions for velocity moments.

3. In these simulations the turbulence was driven by a steady forcing function **F**. The generality of the results is not clear until we explore further the effect of the magnitude and spectral distribution of **F**. Also, do the initial conditions matter? However there are encouraging signs of agreement with other kinds of simulations and with measurements. These comparisons need to be pursued.

4. The computations have given rise to some important new physical ideas; the connection between the advection of small eddies and the advection of small scale pressure fluctuations; the structure of the large scale pressure field; and, finally, perhaps some insight into the temporal pattern of the movement and decay of small scale eddies.

5. There will be several applications of these computations to other areas of turbulence research, including practical applications. It will be possible to compute the effects of turbulence on the generation of internal and surface waves, and to develop representations of the space-time structure of turbulence, either as a 3-D stochastic field, or by means of conditional eddy techniques. Such representations are being used to compute the motions of particles in turbulent flows, where it is too expensive to use direct simulations.

Acknowledgments

We are grateful for very useful suggestions from Dr. R. S. Rogallo of NASA Ames, and from Dr. R. H. Kraichnan who was a visitor to the C.T.R. summer program.

Table 1

Numerical and physical parameters

Number of mesh points: 64^3

Number of time samples: 288

Total disk storage used: 604 Mbytes

Boxsize: 2π

Force field: $F' = \left[\frac{1}{(2\pi)^3}\int |\mathbf{f}|^2 d\mathbf{x}\right]^{1/2} = 0.69$

Kinematic viscosity: $\nu = .02$

Properties of flow field

Velocity field: $\frac{1}{2}\overline{u_i^2} = 1.94$

$u_0 = \left(\frac{1}{3}\overline{u_i^2}\right)^{1/2} = 1.14$

Lengthscale: $L_1 = \frac{3\pi}{4}\int_0^\infty k^{-1}E(k)dk \Big/ \int_0^\infty E(k)dk = 1.25$

Taylor microscale: $\lambda = \left[5\int_0^\infty E(k)dk \Big/ \int_0^\infty k^2 E(k)dk\right]^{1/2} = 0.84$

Kolmogorov microscale: $\ell_{\mathrm{Kol}} = \left(\nu^3/\epsilon\right)^{1/4} = 0.064$

Reynolds number: $Re_\lambda = u_0\lambda/\nu = 48$

Dissipation rate: $\epsilon/(u_0^3/L_1) = (15/Re_\lambda)(L_1/\lambda) = 0.47$

Skewness: $\frac{1}{3}\sum_{i=1}^{3}\overline{\left(\frac{\partial u_i}{\partial x_i}\right)^3} \Big/ \left[\overline{\left(\frac{\partial u_i}{\partial x_i}\right)^2}\right]^{3/2} = -0.50$

Normalized force: $F'L_1/u_0^2 = 0.66$

'Integral' length scales estimated from 1-D correlations:

Velocity: $L_{11}^{(1)}/L_1 = 1.25, \qquad L_{22}^{(1)}/L_1 = 0.76$

Pressure: $L_{pp}^{(1)}/L_1 = 0.75$

'Integral' time scales: $T_1^{(E)}/(L_1/u_0) = 1.5$

$T_2^{(E)}/(L_1/u_0) = 1.3$

REFERENCES

BATCHELOR, G. K. 1951 *Proc. Camb. Phil. Soc.*, **47**, 359-374.

CARRUTHERS, D. J. & HUNT, J. C. R. 1986 *J. Fluid Mech.*, **165**, 475-501.

DURBIN, P. A. & HUNT, J. C. R. 1980 *J. de Macanique*, **19**, 679-95.

FAVRE, A. J., CRANGLIO, J. J. & DUMAS, R. 1956 *J. Fluid Mech.*, **2**, 313-342.

GEORGE, W. K., BEUTHER, P. D. & ARNDT, R. E. A. 1984 *J. Fluid Mech.*, **148**, 155-191.

HINZE, J. O. 1975 Turbulence . *McGraw-Hill, New York.*

LESLIE, D. C. 1981 Developments in the Theory of Turbulence . *Oxford University Press.*

MONIN A. S. & YAGLOM, A. M. 1971 Statistical Fluid Mechanics, vol. 2 . *M.I.T. Press.*

MOSER, R. D. & MOIN, P. 1984 Direct numerical simulations of curved channel flow . *NASA TM 85974.*

MOIN, P. 1987 *AIAA paper 87-0194.*

MOIN, P., ADRIAN, R. J. & KIM, J. 1987 Stochastic estimation of the structure in turbulent channel flow . 6th *Symposium on Turbulent Shear Flows, Toulouse.*

ROGALLO, R. S. 1981 Numerical experiments in homogeneous turbulence . *NASA TM 81315.*

SABOT, J. & COMTE-BELLOT, G. 1976 *J. Fluid Mech.*, **74**, 767-796.

SHLIEN, D. J. & CORRSIN, S. 1974 *J. Fluid Mech.*, **62**, 255-271.

SNYDER, W. H. & LUMLEY, J. L. 1971 *J. Fluid Mech.*, **48**, 41-71.

TENNEKES, H. 1975 *J. Fluid Mech.*, **67**, 561.

TENNEKES, H. & LUMLEY, J. L. 1979 A first course in turbulence 2nd edition . *M.I.T. Press*

TOWNSEND, A. A. 1976 Structure of turbulent shear flow 2nd edition . *Cambridge University Press.*

TURFUS, C. & HUNT, J. C. R. 1987 In *Advances in Turbulence*, ed. G. Comte-Bellot & J. Mathieu.

WILLS, J. A. B. 1971 *J. Fluid Mech.*, **20**, 417-432.